第 30 卷第 8 期
2014 年 8 月

无 机 化 学 学 报
CHINESE JOURNAL OF INORGANIC CHEMISTRY

Vol.30 No.8
1977-1984

熔融浸渍法合成单晶锰酸锂作为锂离子电池阴极材料

余 琦[1] 田建华*,[1] 冯明燕[1] 单忠强[1] 崔 兰[2]

([1]天津大学化工学院,天津 300072)

([2]天津大学分析测试中心,天津 300072)

摘要:以二氧化锰和氢氧化锂为原料,通过熔融浸渍法合成具有尖晶石构型的单晶锰酸锂。前驱体 β-MnO_2 以乙酸锰和过硫酸钠为原料通过水热反应合成。基于 TGA/DTA 测试,确定了单晶锰酸锂的煅烧温度为 470 ℃预烧 5 h,再升温至 750 ℃保温 12 h。XRD,FTIR 和 SEM 结果表明,合成的单晶锰酸锂具有均一的棒状结构以及良好的结晶性。电化学性能测试结果表明材料在 0.1C 倍率下充放电时,其首次放电比容量可达 126 mAh·g^{-1},且在一百次循环之后容量保持率为 91%。

关键词:锂离子电池;锰酸锂;单晶;熔融浸渍法

中图分类号:O614.111;O614.7+11 **文献标识码**:A **文章编号**:1001-4861(2014)08-1977-08

DOI:10.11862/CJIC.2014.258

Melt-Impregnation Synthesis of Single Crystalline Spinel $LiMn_2O_4$ Nanorods as Cathode Materials for Li-Ion Batteries

YU Qi[1] TIAN Jian-Hua*,[1] FENG Ming-Yan[1] SHAN Zhong-Qiang[1] CUI Lan[2]

([1]*School of Chemical Engineering and Technology, Tianjin University, Tianjin* 300072, *China*)

([2]*Analysis and Testing Center, Tianjin University, Tianjin* 300072, *China*)

Abstract: The single crystalline spinel $LiMn_2O_4$ was synthesized by melt-impregnation method with the precursor β-MnO_2 and LiOH. The β-MnO_2 was prepared from $Mn(CH_3COO)_2\cdot 4H_2O$ and $Na_2S_2O_8$ by hydrothermal reaction. Based on TGA/DTA analysis, the optimal calcination temperature is fixed at 470 ℃ for 5 h followed by 750 ℃ for 12 h. The inuence of the sintering process on properties of single crystalline $LiMn_2O_4$ was also investigated. XRD, FTIR and SEM results demonstrate the uniform particles and good crystallinity of single crystalline spinel $LiMn_2O_4$ nanorods. The single crystalline $LiMn_2O_4$ obtained by Melt-impregnation method exhibits a superior electrochemical performance, which delivers an initial specific capacity of 126 mAh·g^{-1} and 91% capacity retention at the 100th cycle in the potential range of 3.0 to 4.4 V (vs Li/Li^+).

Keywords: Li-ion battery; $LiMn_2O_4$; single crystalline; melt-impregnation method

0 Introduction

Looking for green renewable resources to replace non-renewable resources is essential in 21st century because of the worldwide energy shortage. Li -ion batteries, owing to their high energy density, light weight, and long cycle life, have been regarded as one of the near-term solutions[1-3]. However, the reported Li -ion technologies fall short of meeting the electric vehicles′ requirement of higher charge-discharge rate capability. Therefore, it is highly desirable to develop the materials and systems of the high performance Li-

收稿日期:2014-01-17。收修改稿日期:2014-03-21。

国家高技术研究发展计划(No.2013AA050901)资助项目。

*通讯联系人。E-mail:jhtian@tju.edu.cn

ion battery[4-6].

Spinel $LiMn_2O_4$ is a promising candidate to replace layered Ni or Co oxide materials as the cathode in Li-ion batteries due to its low cost, environmental friendliness, high abundance, and better safety[7-8]. Besides, the spinel $LiMn_2O_4$ also has good ion transmission channel because of its three-dimensional crystal structure[9-10].

Traditional polycrystalline $LiMn_2O_4$ materials are usually prepared by solid-state reaction with electrolytic manganese dioxide and lithium sources as raw materials[11-13]. Ye et al[14] used Li_2CO_3 and commercial MnO_2 as raw materials to synthesize spinel $LiMn_2O_4$ at 500 ℃ after a ball-milling promoted solid-state reaction. However, the synthesized spinel $LiMn_2O_4$ shows significant capacity fading and poor cycleability when it is cycled over a wide voltage range for increasing the energy density. Two reasons have been considered as the main sources for the capacity fading, one is the dissolution of Mn^{3+} by the disproportional reaction $2Mn^{3+} \longrightarrow Mn^{4+}+Mn^{2+}$, and the other is the generation of new phases during cycling and the related micro-strains[15-17].

Recently, researchers have tried many ways to solve the problem of capacity fading during cycles of spinel $LiMn_2O_4$. Single crystalline $LiMn_2O_4$ with the same space lattice in the three-dimensional plays an important role in solving this problem. Firstly, it can improve the two-phase stability in the high voltage region for lithium ion insertion/extraction. Additionally, single crystalline $LiMn_2O_4$ with the long-range ordered structure can reduce the obstacle in the lithium ion insertion/extraction. The single crystalline primary particles with the nanostructure have also been shown to enhance power performance due to suitable surface-to-volume ratio determined by the morphology of nanorods[18-20]. Up to now, researchers have already synthesized the single crystalline $LiMn_2O_4$ by a variety of methods. Ding et al[19] synthesized single crystalline $LiMn_2O_4$ by calcining the mixture of the precursor and lithium source. In order to obtain the good morphology of nanotube, a template-engaged reaction was used in their work. The first discharge capacity of the obtained single crystalline $LiMn_2O_4$ is about 115 $mAh \cdot g^{-1}$ at 0.1C. In addition, Tang et al [20] used a LiCl-$Mn(NO_3)_2$ system to synthesize single crystals of spinel $LiMn_2O_4$. In order to obtain the uniform fine single crystals of $LiMn_2O_4$, a series of reaction temperature and time during calcination step were investigated in their work. All above methods can synthesize relatively fine single crystals of $LiMn_2O_4$, but cumbersome steps and poor cycle life always exist in their work.

Different from the above preparation methods, a simple synthesis method for producing single crystalline $LiMn_2O_4$ nanorods as cathode material for Li-ion secondary batteries has been studied in this article. Instead of commercial MnO_2, the single crystalline β-MnO_2 nanorods synthesized by hydrothermal method are used as precursor. The influence of the reaction time and temperature on the morphology, particle size and properties of the precursor has been studied. Then, the melt-impregnation method which is simple and requires neither ball-milling nor grinding has been adopted to synthesize single crystalline $LiMn_2O_4$ nanorods. In this process, the molten LiOH is totally absorbed into the lattice of β-MnO_2, leading to a homogeneous mixture. The obtained single crystalline $LiMn_2O_4$ with the well crystallinity and morphology exhibits a superior electrochemical performance.

1 Experimental

1.1 Synthesis of single crystalline $LiMn_2O_4$ nanorods

The synthesis of β-MnO_2 nanorods was carried out by a hydrothermal method[21]. All the chemical reagents were analytical grand and used without further purification. In a typical synthesis, $Mn(CH_3COO)_2 \cdot 4H_2O$ and $Na_2S_2O_8$ were dissolved with a molar ratio of 1:1 in 80 mL of distilled water by magnetic stirring at room temperature to form a homogeneous clear solution. The mixed solution was then transferred into a 100 mL Teflon-lined stainless steel autoclave, sealed and heated in a preheated electric oven for hydrothermal reaction at 120 ℃ for 10 h. After the reaction completed, the autoclave was taken out and

naturally cooled to room temperature. The obtained black precipitated products were washed with distilled water several times by centrifugation to remove excess ions. The obtained powders were dried at 100 ℃ in air over night.

In a typical synthesis of $LiMn_2O_4$ nanorods: as-synthesized β-MnO_2 nanorods and LiOH with a suitable molar ratio in stoichiometric were mixed to form a mixture. Then the product was obtained by the melt-impregnation method without grinding. The mixed powders were precalcined in air to make the molten state lithium into the lattice of the β-MnO_2, and from a well-mixture. Then the well-mixture was heated to a relatively high temperature for further sintering.

1.2 Determined of the reaction condition of single crystalline $LiMn_2O_4$

We adjusted some common hydrothermal treatment conditions such as reaction time (8, 10, 12, 14 h) and temperature (100, 120, 140, 160 ℃) to obtain single crystal β-MnO_2 nanorods. The molten LiOH at 470 ℃ for 5 h was totally absorbed into the lattice of β-MnO_2, leading to a homogeneous mixture, and then heated to 750 ℃ and held for 12 h.

1.3 Physicochemical characterization

The nanostructure and crystalline of β-MnO_2 and $LiMn_2O_4$ were characterized by X-ray diffraction (XRD, D/MAX-2500, Japan) analysis using Cu $K\alpha$-radiation (λ=0.154 18 nm) between 10° and 90° at 40 kV and 20 mA. TGA test was performed to investigate the calcination temperature on Q500V20.10 Build 36 from 0 ℃ to 800 ℃ with a heating rate of 10 ℃·min^{-1}. The morphology and size of the prepared nanostructure β-MnO_2 and $LiMn_2O_4$ were analyzed by S-4800 field emission scanning electron microscopy (FESEM, Hitachi S-4800, accelerating voltage of 15 kV, Japan). High-resolution transmission electron microscopy (HRTEM) and selected-area electron diffraction (SAED) were collected on JEM-2100F with an accelerating voltage of 200 kV. A Fourier transform infrared spectrometer (FT-IR, Avatar360) was used to study the structure coordination of the precursor and single crystalline $LiMn_2O_4$.

1.4 Electrochemical investigation

The electrodes for electrochemical studies were prepared by mixing 80wt% $LiMn_2O_4$ as the active material, 10wt% carbon black (Vulcan-72, Cabot Co., USA) as the conductive agent, and 10wt% polytetrafluoroethylene as the binder. A small quantity of ethanol was used to mix the three components followed by an ultrasonication treatment for 30 min. Then the slurry was coated onto an aluminum foil current collector and dried at 100 ℃ for 12 h in a vacuum oven. The coated cathode foil was then pressed to form a uniform layer and punched in the form of a round disk with a 14 mm diameter. The cathode was performed using CR2032 coin-type cells which were assembled in a glove box filled with argon. Lithium metal foil was used as the anode, a 1 mol·L^{-1} solution of $LiPF_6$ in ethylene carbonate/diethyl carbonate (EC/DEC, 1∶1, *V*/*V*) was used as the electrolyte with a microporous polypropylene film (Celgard 2000) as the separator. The charge-discharge cycle tests were performed at various C rates between 3.0 and 4.4 V (vs Li/Li^+) by a land battery test system (CT-2001) at room temperature. Cyclic Voltammogram (CV) was recorded on LK3200 electrochemical workstation at a scan rate of 0.1 mV·s^{-1} from 3.0 to 4.4 V (vs Li/Li^+). The electrochemical potential changes also can be used to investigate the structural changes during cycles.

2 Results and discussion

2.1 Physicochemical properties of precursor β-MnO_2 and single crystalline $LiMn_2O_4$

All the diffraction peaks in Fig.1a can be readily indexed to the pure tetragonal phase of β-MnO_2 (PDF 24-0735) with $P4_2/mnm$ space group, lattice constants a=0.439 99 nm and c=0.287 40 nm. No peaks for other types of manganese oxides can be observed, indicating that the as-prepared products are phase-pure β-MnO_2 nanorods. The sharp diffraction peaks also reveal that the products are well crystalline ones. All the diffraction peaks on the XRD patterns of Fig.1b can be indexed to a pure face-centered cubic spinel $LiMn_2O_4$ (PDF card No.35-0782), which belongs to the

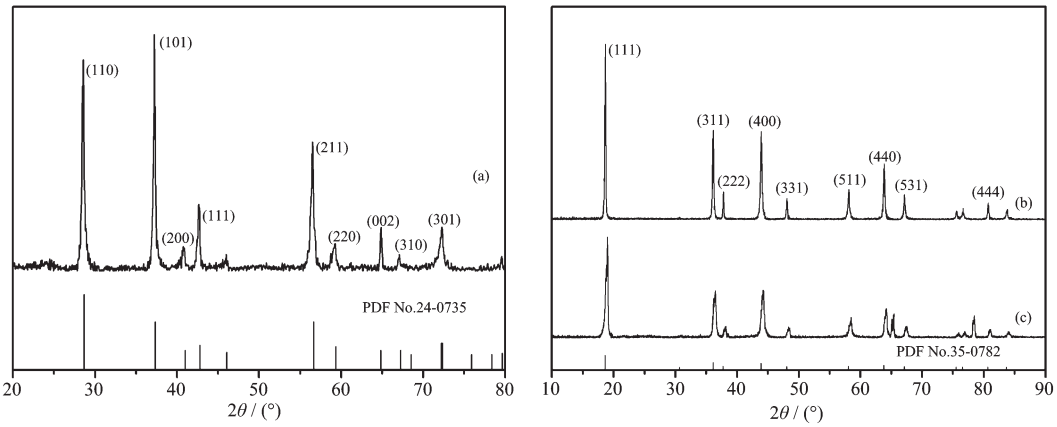

Fig.1 XRD patterns of the as-synthesized (a) β-MnO_2 nanorods as precursor by the hydrothermal method, with the PDF card number at the bottom (b) the single crystalline $LiMn_2O_4$ nanorods as obtained from melt-impregnation method, (c) the single crystalline $LiMn_2O_4$ nanorods after 100 cycles at 0.1C, the PDF card number at the bottom

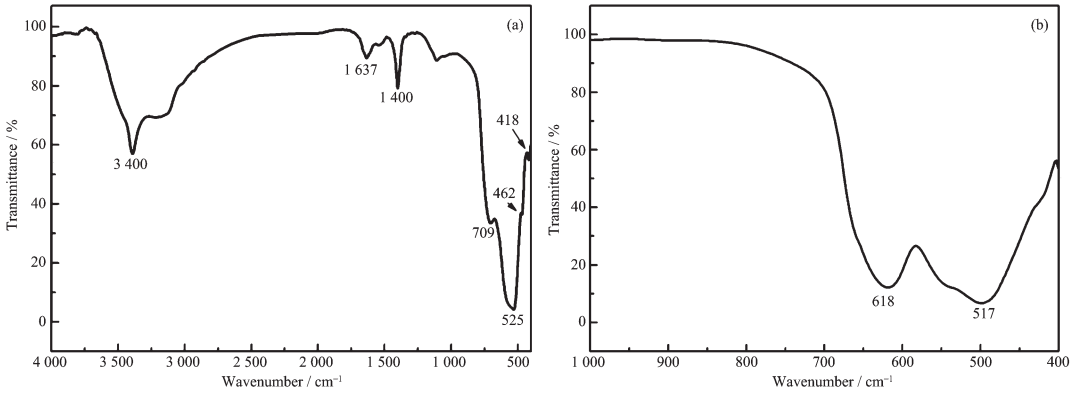

Fig.2 FTIR spectra of (a) β-MnO_2 precursors and (b) single crystalline $LiMn_2O_4$ obtained by the melt-impregnation method

Fd3m space group. No peaks of the β-MnO_2 phase are detected in Fig.1b, demonstrating that the single-phase spinel $LiMn_2O_4$ can be obtained from melt-impregnation method. The XRD pattern of the single crystalline $LiMn_2O_4$ after 100 cycles is shown in Fig. 1c. The good crystallinity of the single crystalline $LiMn_2O_4$ after 100 cycles is maintained with a slight difference in the intensity and sharpness. In short, the single crystalline $LiMn_2O_4$ synthesized by this method has good loop stability and a good crystal structure even after 100 cycles (Fig.1c).

Fig.2 shows the FTIR spectra of the β-MnO_2 precursors and single crystalline $LiMn_2O_4$ nanorods. As shown in Fig.2a, the bands at around 3 400, 1 637 and 1 400 cm^{-1} correspond to the O-H vibrating mode of traces of absorbed water. The bands at about 709, 525, 462 and 418 cm^{-1} can be ascribed to the Mn-O vibrations of the rutile-type MnO_6 octahedra framework, which present a clear signature that can be used for probing the β-MnO_2 type materials. It is noticeable that there are no IR bands related to the Ramsdellite impurity and the results are in good agreement with the published values[22-23]. The FTIR spectra of $LiMn_2O_4$ samples are shown in Fig.2b. The observed high-frequency bands, located around 618 and 517 cm^{-1}, are associated with the asymmetric stretching modes of MnO_6 group. These results are quite similar to those given in earlier reports[24].

In order to determine the reaction temperature of the melt-impregnation method, TGA/DTG (Fig.3) test was performed. As shown in Fig.3b, the peak at 100 ℃ corresponds to the loss of the crystal water in $LiOH \cdot H_2O$. Whereas, LiOH begins to decompose with the temperature increasing to 500 ℃. Thus, we choose the temperature of 470 ℃ being lower than 500 as pretreatment temperature to melt LiOH, which results

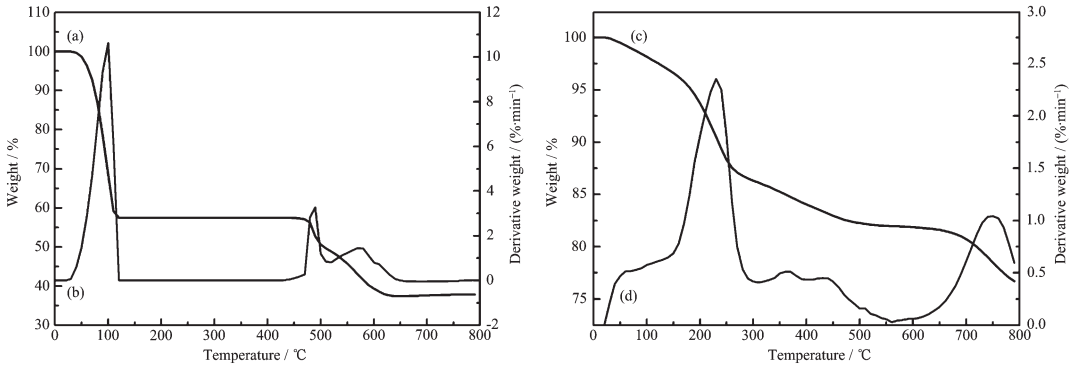

Fig.3　TGA (a)/DTG (b) curves of $LiOH\cdot H_2O$ and the TGA (c)/DTG (d) curves of mixture of $LiOH\cdot H_2O$ and MnO_2

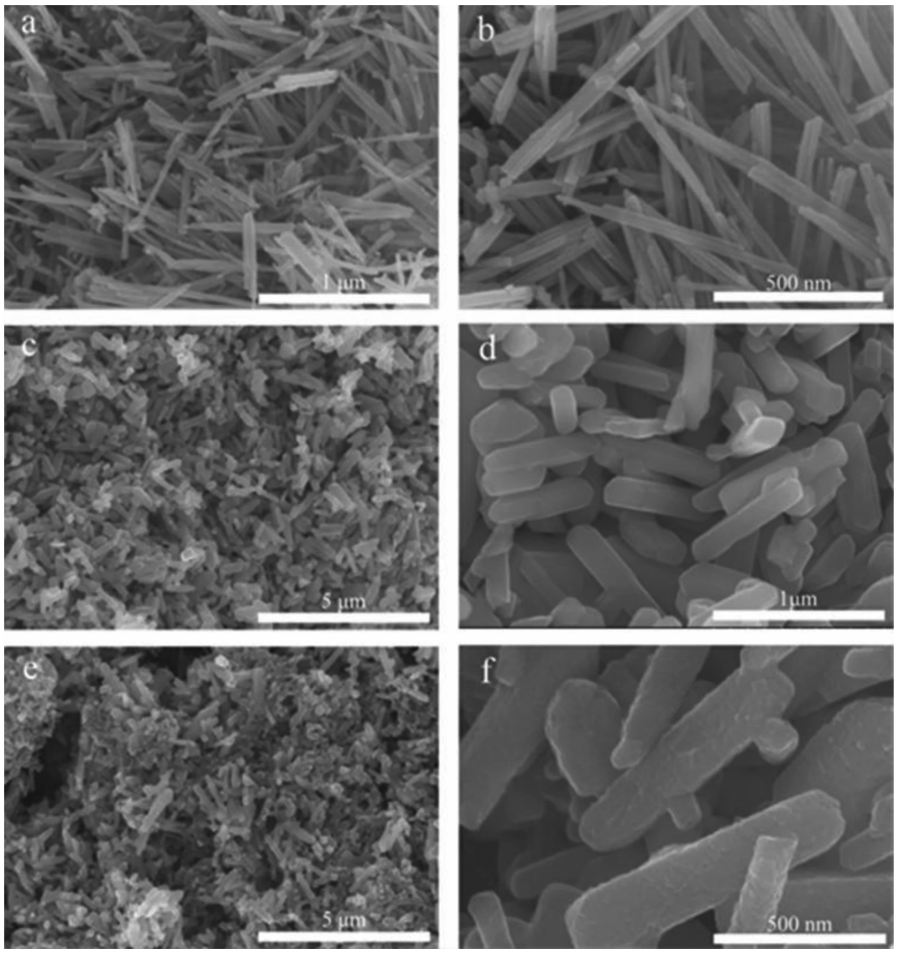

Fig.4　SEM images of (a, b) the precursor β-MnO_2 nanorods with different magnifications, (c, d) the single crystalline $LiMn_2O_4$ nanorods with different magnifications, (e, f) the single crystalline $LiMn_2O_4$ nanorods after 100 cycles at 0.1C with different magnifications

in well mixing of molten LiOH with β-MnO_2. However, the thermal decomposition of the mixture of $LiOHH_2O$ and MnO_2 occurs at 200 ℃ (Fig.3c and d). The weightlessness also can be observed between 300 and 500 ℃. In addition, another weightlessness is observed over 650 ℃, which is probably due to the formation of $LiMn_2O_4$[25]. And when the temperature increases to 750 ℃, the rate of the weight loss is the maximum. Therefore, 470 ℃ is determined as the pretreatment temperature, and the calcination temperature is 750 ℃.

As is shown in Fig.4a and b, all of the β-MnO_2 samples are well dispersed with average diameter 20~

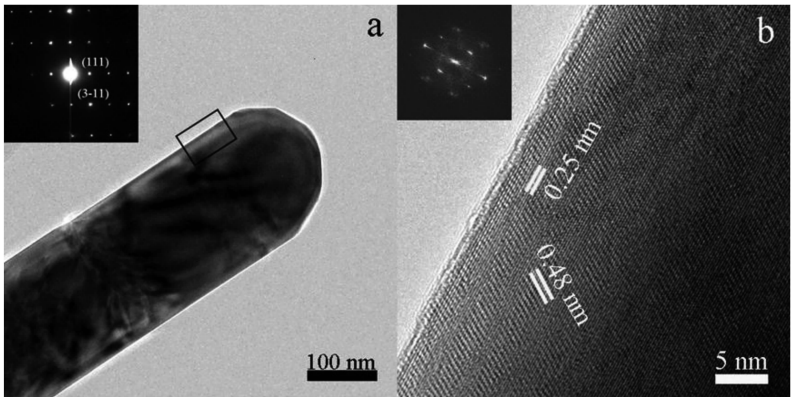

Fig.5 (a) TEM micrograph of single crystalline $LiMn_2O_4$; Inset, the selected-area electrode diffraction (SAED) pattern; (b) HRTEM micrograph (obtained from rectangular box in Fig.5a) of single crystalline $LiMn_2O_4$; Inset: the fast Fourier transform (FFT) pattern

30 nm and lengths of several micrometers. Fig.4c and d show the SEM images of the single crystalline $LiMn_2O_4$ obtained from melt-impregnation method. Obviously, the high quality cubic spinel $LiMn_2O_4$ nanorods are well-dispersed and mainly maintain the morphology of nanorods, but a wider average diameter of 160 nm and a shorter average length of 650 nm comparing to those of the precursor β-MnO_2 nanorods. Fig.4e and f show the images of the single crystalline $LiMn_2O_4$ nanorods after 100 cycles at 0.1C, which exhibits that the single crystalline $LiMn_2O_4$ still maintains good morphology of nanorods, indicating the well stability of the materials during the cycles.

Fig.5 shows a representative TEM micrograph of the single crystalline $LiMn_2O_4$. The selected-area electron diffraction (SAED) pattern (Fig.5a, inset), in which a series of dots array in a line and every dot can be seen clearly without diffraction rings, implying a single-crystal structure[26]. A HRTEM (Fig.5b) of single crystalline $LiMn_2O_4$ extracted from Fig.5a shows that the (111) and (311) atomic planes with a lattice spacing of 0.48 nm and 0.25 nm, respectively. The obtained nanorods grow along the [111] crystallographic direction, increasing the abundance of the (311) plane. Additionally, the FFT pattern in inset of Fig.5b also suggests that nanorods are single crystalline.

2.2 Electrochemical performance of single crystalline $LiMn_2O_4$

Coin-type cell configuration was used to evaluate the electrochemical properties of the materials as cathode electrode. First charge-discharge curve of single crystalline $LiMn_2O_4$ nanorods at 0.1C (14.8 $mAh \cdot g^{-1}$) in the potential range of 3.0~4.4 V (vs Li^+/Li) is shown in Fig.6a. The discharge curve exhibits two undistinguished plateaus at around 3.9 and 4.1 V, which indicates the charge/discharge signature of the lithium-rich spinel structure[7,27]. The single crystalline $LiMn_2O_4$ with this characteristic is also generally expected to have better cycle performance as a cathode electrode material than the normal stoichiometric one. The charge capacity is about 132 $mAh \cdot g^{-1}$, and the discharge capacity is about 126 $mAh \cdot g^{-1}$, showing a high Coulombic efficiency of 95% at first cycle. As shown in Fig.6b, the discharge capacities are around 126, 115, 110 $mAh \cdot g^{-1}$ for the first cycle when the cell is cycled at 0.1C, 1C and 2C, respectively. To further investigate the cycle performance of single crystalline $LiMn_2O_4$ nanorods, the cell was cycled at 0.1C, 1C and 2C for 100 cycles (Fig. 6c). As is shown in Fig.6c, the discharge capacity of $LiMn_2O_4$ nanorods shows very well capacity retention at various current rates. The discharge capacity is above 105 $mAh \cdot g^{-1}$ at 0.1C, and keeps a 90% capacity after 100 cycles, which is similar to 1C. When the current rates increase to 2C with a 1C charge rate, the discharge capacity drops to the 110 $mAh \cdot g^{-1}$ at the first cycle, but after 100 cycles there is also 100 $mAh \cdot g^{-1}$ left, showing a 91% capacity retention, and a 99% coulomb efficiency over cycles. The rate capability of single crystalline $LiMn_2O_4$

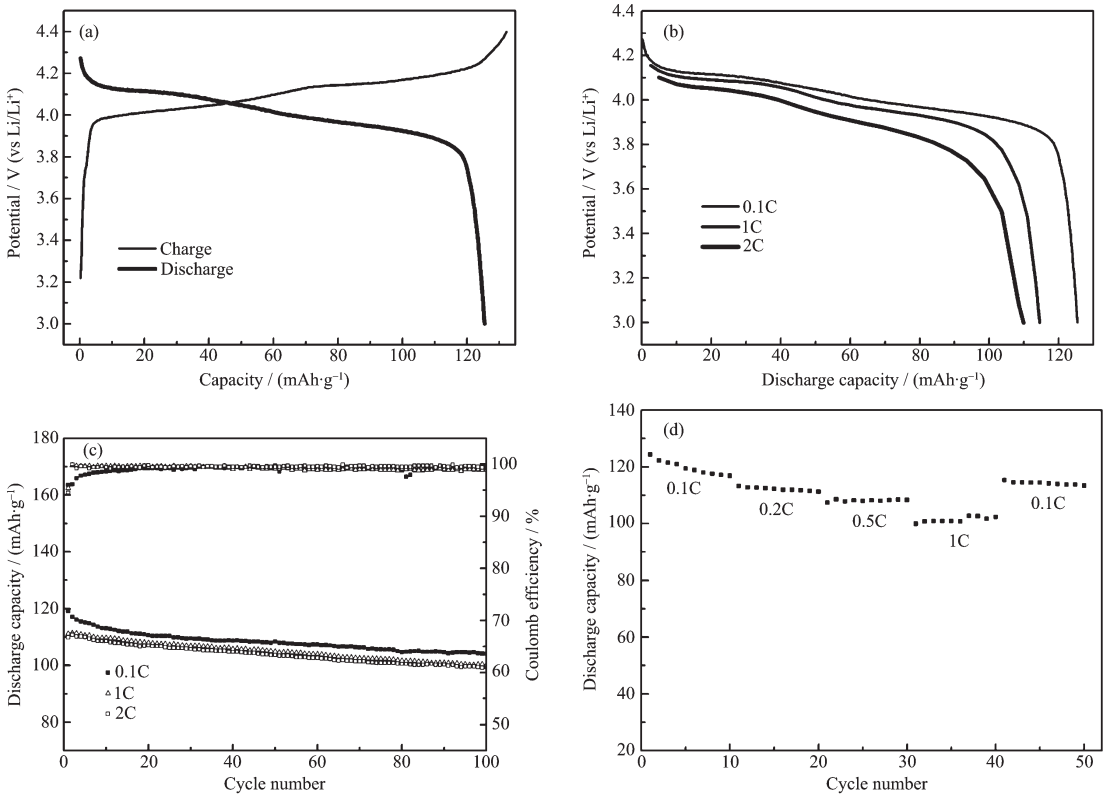

Fig.6　(a) First charge-discharge curves at 0.1C (b) Discharge curves at different rates (c) Cyclic performance at 0.1C, 1C and 2C for 100 cycles and corresponding coulomb efficiency (d) Discharge capacity with cycling number at different current rates of single crystalline $LiMn_2O_4$

nanorods varying from 0.1C to 1C rate is shown in Fig.6d. After ten cycles at 0.1C, the rate is increased in stages to 1C. The discharge capacity of single crystalline $LiMn_2O_4$ fades from 125 mAh·g^{-1} to 102 mAh·g^{-1} when the current rates increase from 0.1C to 1C, respectively. After high rate measurement, the cell with the cathode of single crystalline $LiMn_2O_4$ is still able to supply the previously measured value at 0.1C, an indication of the high reversibility of the system. This also precisely shows a good stability of single crystal structure. All the evidences above exhibit the excellent electrochemical properties of the single crystalline primary particles of $LiMn_2O_4$. The small particle size of single crystalline $LiMn_2O_4$ could reduce the lithium ion diffusion path and the loss of Li^+ in the insertion/extraction, thus has a good cycle life. And these advantages could be attributed to the one-dimensional electron transport and large specific surface area of the single crystalline nanorods. Therefore, the products obtained above confirm that the method described here could be employed as a rational route to synthesize high rate, high crystallinity spinel $LiMn_2O_4$ with single crystalline nanorod structure.

Fig.7 shows the cyclic voltammetry (CV) curves of single crystalline $LiMn_2O_4$ between potential limits of 3.0 and 4.5 V (vs Li^+/Li) at a scanning rate of 0.1 mV·s^{-1}. The charge stage has two sharp peaks at around 4.07 and 4.18 V, and the discharge stage also shows two sharp peaks at around 3.95 and 4.08 V vs Li^+/Li, which correspond with the two undistinguished plateaus of Fig.6a. The two pairs of redox peaks in the CV curves suggest that lithium ions extract from and insert into spinel structure by a two-step process, which is in good agreement with those typical well-crystallized spinel $LiMn_2O_4$[28-29]. In addition, Fig.7 also shows that the absolute value ratio of the oxidation peak current and the reduction peak is almost equal, which indicates that the reaction is highly reversible. In addition, the peak position and peak intensity only change a little in the case of the $LiMn_2O_4$ cathode for

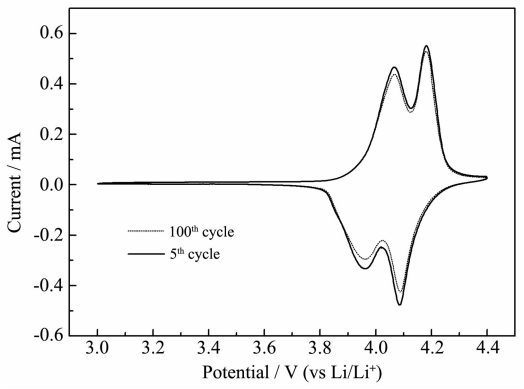

Fig.7 Cyclic voltammetry (CV) curves of single crystalline $LiMn_2O_4$ at a scanning rate of 0.1 $mV \cdot s^{-1}$

the various cycles, indicating only small polarization occurrence in the surface of electrode and the structural stability of single crystalline primary particles.

3 Conclusions

In conclusion, we have demonstrated a very simple and cost effective approach for fabrication of highly ordered single crystalline $LiMn_2O_4$ nanorods. It turns out that the mixtures of β-MnO_2 nanorods and LiOH prepared by melt-impregnation method are more uniform than those prepared by solid-state reaction method[10-13]. The results of XRD, SEM and FTIR confirm that the obtained single crystalline $LiMn_2O_4$ has good morphology and well ctystallinity. HRTEM and SAED analysis reveal that $LiMn_2O_4$ has a regular lattice arrangement and specific characteristics of single crystal, which is very important in improving the kinetic properties of the material. The single crystalline $LiMn_2O_4$ is able to deliver 115 $mAh \cdot g^{-1}$ at a high current rate of 1C (126 $mAh \cdot g^{-1}$ at 0.1C) and has a high reversibility and good capacity retention after 100 cycles. All of these prove that the outstanding electrochemical performance of single crystalline $LiMn_2O_4$ owes to such synthesis method.

References:

[1] Xu B, Qian D, Wang Z, et al. *Mater. Sci. Eng. R*, **2012**,**73**(5):51-65

[2] Tang W, Liu L L, Tian S, et al. *Electrochem. Commun.*, **2011**,**13**(11):1159-1162

[3] Yang Y, Xie C, Ruffo R, et al. *Nano Lett.*, **2009**,**9**(12):4109-4114

[4] Deng Y, Zhou Y, Shi Z, et al. *J. Mater. Chem. A*, **2013**,**1**:8170-8177

[5] Whittingham M S. *Chem. Rev.*, **2004**,**104**(10):4271-4301

[6] Kang K, Meng Y S, Breger J, et al. *Science*, **2006**,**311**(5763):977-980

[7] Luo J Y, Xiong H M, Xia Y Y. *J. Phys. Chem. C*, **2008**,**112**(31):12051-12057

[8] Lee H W, Muralidharan P, Ruffo R, et al. *Nano Lett.*, **2010**,**10**(10):3852-3856

[9] Hu D H, Zhao S X, Deng Y F, et al. *J. Mater. Chem. A*, **2013**,**1**(46):14729-14735

[10]Wang F X, Xiao S Y, Gao X W, et al. *J. Power Sources*, **2013**,**242**:560-565

[11]Yue H J, Huang X K, Lü D P, et al. *Electrochim. Acta*, **2009**,**54**(23):5363-5367

[12]Luo J, Wang Y, Xiong H, et al. *Chem. Mater.*, **2007**,**19**(19):4791-4795

[13]Li T, Qiu W H, Zhao H L, et al. *Mater. Lett.*, **2006**,**60**(9):1251-1255

[14]Ye S H, Lü J Y, Gao X P, et al. *Electrochim. Acta*, **2004**,**49**(9):1623-628

[15]Aurbach D, Levi M D, Gamulski K, et al. *J. Power Sources*, **1999**,**81**:472-479

[16]Xia Y, Zhou Y, Yoshio M. *J. Electrochem. Soc.*, **1997**,**144**(8):2593-2600

[17]Shin Y, Manthiram A. *J. Electrochem. Soc.*, **2004**,**151**(2):A204-A208

[18]Kim D K, Muralidharan P, Lee H W, et al. *Nano Lett.*, **2008**,**8**(11):3948-3952

[19]Ding Y L, Xie J, Cao G S, et al. *Adv. Funct. Mater.*, **2011**,**21**(2):348-355

[20]Tang W, Yang X, Liu Z, et al. *J. Mater. Chem.*, **2002**,**12**(10):2991-2997

[21]Wang X, Li Y. *J. Am. Chem. Soc.*, **2002**,**124**(12):2880-2881

[22]Potter R M, Rossman G R. *Am. Mineral.*, **1979**,**64**(11/12):1219-1226

[23]Gao T, Fjellvg H, Norby P. *Nanotechnology*, **2009**,**20**(5):055610

[24]Wang G G, Wang I M, Mao W Q, et al. *J. Solid State Electrochem.*, **2005**,**9**(7):524-530

[25]Kong X Y, Ding Y, Yang R, et al. *Science*, **2004**,**303**(5662):1348-1351

[26]Li Z, Wang L, Li K, et al. *J. Alloys Compd.*, **2013**,**580**:592-597

[27]Xia Y, Yoshio M. *J. Electrochem. Soc.*, **1997**,**144**(12):4186-4194

[28]Xia Y, Yoshio M. *J. Electrochem. Soc.*, **1996**,**142**(3):825-833

[29]Ohzuku T, Kitagawa M, Hirai T. *J. Electrochem. Soc.*, **1990**,**137**(3):769-775